JCTC Journal of Chemical Theory and Computation

Article

pubs.acs.org/JCTC

Molecular Dynamics Studies of Liposomes as Carriers for Photosensitizing Drugs: Development, Validation, and Simulations with a Coarse-Grained Model

Joakim P. M. Jämbeck,[†] Emma S. E. Eriksson,[‡] Aatto Laaksonen,[†] Alexander P. Lyubartsev,[†] and Leif A. Eriksson*,[‡]

[†]Division of Physical Chemistry, Arrhenius Laboratory, Stockholm University, SE-10691, Stockholm, Sweden

[‡]Department of Chemistry and Molecular Biology, University of Gothenburg, SE-41296 Göteborg, Sweden

Supporting Information

ABSTRACT: Liposomes are proposed as drug delivery systems and can in principle be designed so as to cohere with specific tissue types or local environments. However, little detail is known about the exact mechanisms for drug delivery and the distributions of drug molecules inside the lipid carrier. In the current work, a coarse-grained (CG) liposome model is developed, consisting of over 2500 lipids, with varying degrees of drug loading. For the drug molecule, we chose hypericin, a natural compound proposed for use in photodynamic therapy, for which a CG model was derived and benchmarked against corresponding atomistic membrane bilayer model simulations. Liposomes with 21−84 hypericin molecules were generated and subjected to 10 microsecond simulations. Distribution of the hypericins, their orientations within the lipid bilayer, and the potential of mean force for transferring a hypericin molecule from the interior aqueous "droplet" through the liposome bilayer are reported herein.

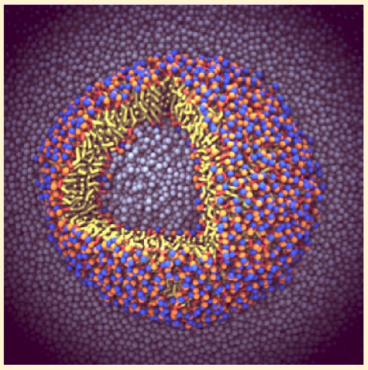

INTRODUCTION

The antitumor activity of hypericin, a napthodianthrone isolated from *Hypericum perforatum*,[1] has been documented in both in vivo[2−4] and in vitro studies.[5−7] It has also been shown that hypericin possesses antiviral properties against viruses such as human immunodeficiency virus (HIV)[8−10] and hepatitis B.[11] The light-absorbing properties furthermore makes this molecule an efficient photosensitizer with the potential to be used in photodynamic therapy (PDT). Three components are necessary for the PDT procedure: light, the administrated drug, and oxygen. When the area where the drug has been administrated is irradiated with light, the photosensitizer absorbs a photon and via intersystem crossing reaches the excited triplet state. In the presence of O_2, the excitation energy is transferred, which generates singlet oxygen and possibly other reactive oxygen species (ROS). The exact cellular target for hypericin remains unknown, and the mechanism of transport is yet to be elucidated. Some studies have suggested that hypericin due to its hydrophobicity prefers to accumulate in the membrane of the cell or one of the organelles or a membrane-bound protein.[12,13] This indicates that hypericin enters the cells via diffusion over the cell membrane, and it is likely that carriers such as low-density lipoproteins can assist in distributing the molecules.[3,14,15] As the drug should be transported directly to the tumorous area, the delivery system of the drugs is of importance. One way of increasing the accumulation of hypericin in the desired area could be to use liposomes packed with hypericin or other photoactive compounds. Liposomes are artificially prepared vesicles composed of lipid molecules that can transfer hydrophobic or sensitive compounds to the cells.[16,17] This approach has been tested for use in PDT and showed promising results.[18,19]

An atomistic picture of how hypericin interacts with cell membranes and how the delivery from a liposome carrier to an actual membrane takes place is difficult to obtain in experimental studies due to thermal fluctuations of soft matter. An emerging area of research that can offer detailed information of how molecules interact on an atomistic scale is molecular simulations. Usually molecular dynamics (MD) or Monte Carlo simulations are used to obtain structural and dynamic information. Despite the clear advantage (from a resolution point of view) of using atomistic models when simulating liposomes or vesicles, only a few studies have employed such detailed models due to the computational efforts needed, although some landmark work has been reported.[20−22] In previous work of our group, we have studied the thermodynamics of incorporating hypericin and relevant derivatives in model membranes at atomistic resolution,[23,24] but no simulations on larger scale of hypericin and liposomes have been performed. The prohibiting factors, while simulating large biological systems, are the system sizes and time scales. To properly sample the relevant parts of phase space, very long simulations are needed (microseconds to milliseconds or even longer).[25] Coarse-grained (CG) modeling aims at decreasing the number of particles in the system while still keeping the

Received: June 4, 2013
Published: December 5, 2013

general physics of the model correct. This dimension reduction facilitates longer simulations of larger, often more biologically relevant, systems than fully atomistic ones. A popular CG model is Martini[26] that can be used to study different lipid bilayers,[26−28] proteins,[29,30] and carbohydrates.[31] Within this model, three or four heavy atoms plus their bound hydrogens are grouped together and form larger chemical entities, usually referred to as beads. This allows for more efficient exploration of phase space at the price of a slight loss in resolution. The model has been used in several studies regarding liposomes/vesicles,[32−35] lipid rafts,[36−38] and membrane proteins.[39−41] It should be mentioned that also several other CG models,[42−47] and methods to obtain these,[48−52] do exist.

There is a 2-fold objective with our study: (i) create a CG model of hypericin and verify it against more detailed atomistic simulations and (ii) to explore the impact of hypericin on a liposome—how do the molecules affect its structure and stability and how will they be distributed in the liposome? On the basis of the work and findings presented herein, we aim at performing large-scale CG simulations to quantitatively and qualitatively describe the interactions between a drug carrier and a model membrane in order to bring further insight into the actual delivering process.

METHODS AND MODELS

Coarse-Grained Hypericin. Our strategy for creating a CG model of hypericin follows the Martini model[26] by grouping three and four heavy atoms into one CG bead. The reference data for our fitting of the parameters were taken from a previous united atom (UA) study,[23] where the potential of mean force (PMF) of transferring a hypericin from water to the center of a DPPC lipid bilayer was computed. Hence, the aim of the parametrization was to reproduce this PMF. In Figure 1, the coarse-grained model is presented. The polar entities of hypericin, namely, the carbonyl and hydroxyl groups, were assigned according to the standard Martini parameters, SNa and SNda, respectively. Initially, the bead type SC1 was assigned to the hydrophobic parts of the molecule, but initial simulations showed that this underestimated the lipophilicity of the molecule. Therefore, a new bead type was introduced, SC11. The interactions between the new bead type and selected parts of the DPPC lipid were then optimized in order to reproduce the UA PMF as well as possible. To this end, the interactions between SC11 and the Martini bead type SC1 were optimized, whereas the remaining nonbonded interactions between SC11 and the rest of the system were taken to be the same as for SC1. The parameters obtained from the final parametrization can be found in the Supporting Information.

All bonds in the CG model are shown in Figure 1b, and the force constant for each bond was set to 20,000 kJ mol^{-1} nm^{-2}. The bond lengths were set in order to keep the outer dimensions of the molecule close to the ones obtained from the optimized geometry obtained from ab initio calculations employing density functional theory with the B3LYP exchange−correlation functional[53−56] with the 6-31G(*d*,*p*) basis set. To keep the geometry of hypericin, angular and torsional parameters were assigned where necessary (Supporting Information). As hypericin has the ability to adopt a twisted or bent conformation,[57] no bonds between beads R9−R10 and R7−R8 were assigned. Preliminary simulations showed that improper torsional parameters were not necessary to ensure the aromatic structure remained essentially flat, and hence, these terms were not added.

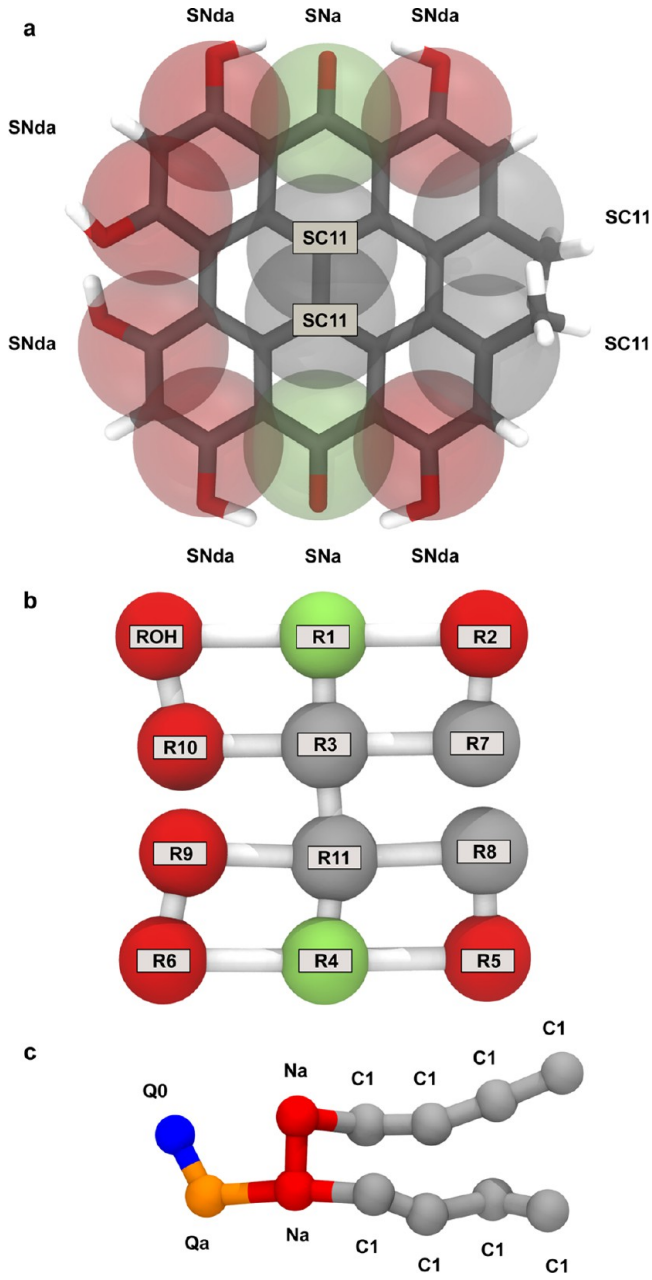

Figure 1. (a) Mapping of coarse-grained beads to the hypericin molecule. Red and green beads correspond to hydrophilic entities and gray beads to hydrophobic ones. Each bead's Martini parameter is given in the boxes. (b) Final coarse-grained model of hypericin, with the name of each bead given in the boxes. (c) DPPC lipid with the Martini model. Molecules in (a) and (b) are shown in the same orientation to facilitate a direct comparison.

Potential of Mean Force Calculations. To compute the PMF of transferring a CG hypericin to the center of a CG DPPC lipid bilayer, umbrella sampling (US)[58] was used. The center of mass (COM) distance between a lipid bilayer consisting of 256 lipids (128 per leaflet) and one hypericin molecule along the membrane normal was chosen as reaction coordinate. These US settings are within the recommendations of Hinner et al.[59] The bilayer was hydrated using 6803 Martini water beads, corresponding to a hydration level of roughly 79 water molecules per lipid. The lipids were modeled with the standard Martini parameters (Figure 1c).[26,27] The reaction

dx.doi.org/10.1021/ct400466m | J. Chem. Theory Comput. 2014, 10, 5−13

coordinate was equally distributed over 98 windows with a 0.05 nm spacing between them. The solute was placed at the desired position by gradually turning on its interactions with the environment according to $U^{\text{inter}}(\lambda) = \lambda U_{\text{A}}^{\text{inter}} + (1 - \lambda)U_{\text{B}}^{\text{inter}}(\lambda)$, where $U_{\text{A}}^{\text{inter}}(\lambda)$ is the potential for the whole system including the solute and $U_{\text{B}}^{\text{inter}}(\lambda)$ is the potential for the bilayer and water alone. The solute was introduced by switching the coupling parameter λ from 0 to 1 with a rate of 1×10^{-7} ps^{-1}. A harmonic potential with a force constant of 1000 kJ mol^{-1} nm^2 was acting on the COM of the solute in order to keep it within the umbrella window. The final snapshots from these simulations were used as starting structures for the production US simulations, which lasted for 1.05 μs per window with the initial 50 ns regarded as equilibration. The reason for the long sampling per US window is due to the slow convergence of the PMF and the possible presence of orthogonal degrees of freedom that has to be sampled properly.[59,60] The weighted histogram analysis method (WHAM)[61] was used to construct the PMF with the g_wham module of the Gromacs simulations package.[62] For all US simulations, the equations of motion were integrated using a stochastic integrator with a coupling period of 1.0 ps to the thermostat in the isothermal−isobaric (*NPT*) ensemble.

Molecular Dynamics Simulations. All simulations were performed in the *NPT* ensemble with the pressure set to 1.013 bar and coupled isotropically with a compressibility of 3×10^{-5} bar^{-1} and temperature set to 323 K. For the bilayer simulations, the pressure in the membrane plane was coupled separately from the pressure in the direction orthogonal to the membrane plane. The temperature and pressure were coupled to baths according to the method described by Berendsen et al.[63] with coupling constants of 1.0 and 5.0 ps, respectively. Electrostatic interactions were shifted in order to smoothly decay to zero while going from 0.0 to 1.2 nm with a dielectric constant of 15. van der Waals interactions were modeled with a Lennard−Jones potential that was shifted from 0.9 to 1.2 nm. Following the advice in a relatively recent debate,[64,65] the neighborlist was kept at a distance of 1.6 nm and was updated every fifth step. A time step of 20 fs was used to integrate the equations of motion with a Leap-Frog integrator. As a CG model introduces an energy landscape with smoother features than its corresponding fully atomistic energy landscape, the interpretation of the time scales is not straightforward. Generally, a 4-fold scaling of the time is advised with the Martini model,[26] and hence, all reported simulation times in the present manuscript are effective ("atomistic") times, meaning that they have been scaled by a factor of 4. Initially, the liposomes were created using the Packmol software package[66] with 947 and 1581 DPPC lipids placed in the inner and outer monolayer, respectively. A total of 8160 water beads were used to hydrate the center of the liposome, and 156,960 additional water beads were used to hydrate the liposome. In Figure 2, a system without hypericin is shown. An initial 1 μs test simulation showed that this liposome construct was stable, and the final snapshot was then used as a starting point for the subsequent simulations of drug loaded systems. In total, six simulations were performed with the number of hypericin molecules ranging from 0 to 84; a summary of all simulations performed is presented in Table 1. In the presence of hypericin, the solutes were placed randomly in the aqueous phase, outside the liposome in all cases except one, and the structures were energy minimized using the steepest descent method. After this, the systems were allowed to relax for 20 ns before the production simulations were initiated.

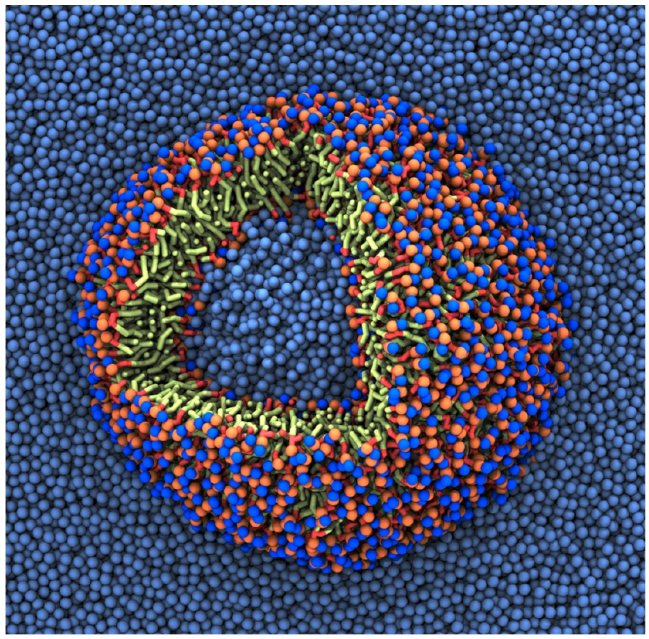

Figure 2. A snapshot from the simulation of a liposome with no hypericin present. Water beads are rendered in blue, phosphorus groups in orange, choline groups in dark blue, glycerol beads in red, and the hydrophobic tails in green. To visualize the cross section and inner part of the liposome, a segment has been cut out.

Table 1. Simulations Performed in the Current Study

name	no. lipids	no. water	no. hypericin	no. CG[a] particles	simulation time[b] (μs)
no hypericin	2528	165,120	0	195,456	10
21 hypericin[c]	2528	165,120	21	195,708	10
21 hypericin	2528	165,120	21	195,708	10
42 hypericin	2528	165,120	42	195,960	10
64 hypericin	2528	165,120	64	196,224	10
84 hypericin	2528	165,120	84	196,464[d]	10

[a]Coarse-grained. [b]Effective simulation time; see text for more details. [c]With one hypericin molecule placed in the middle of the liposome. [d]Corresponding to 2,311,088 atoms.

RESULTS AND DISCUSSION

Parameterization and Validation. *Potential of Mean Force.* In Figure 3, the final PMF is compared to the UA one. The overall shape of the CG PMF is in good agreement with the UA PMF, with the exception of an almost insignificant barrier around z = 3.0 nm. The minima have the same position in both PMFs, which is within the bilayer, close to the lipid/water interface; the only differences are in the depth and slope. The CG model is not able to fully reproduce the UA model, but the difference is small and the pronounced lipophilicity is still evident. As the CG model lacks specific electrostatic interactions, this is to be expected; as in the high density region of the lipid head groups, there are several possibilities for the hypericin molecule to interact with the lipids through hydrogen bonds. Other atomistic simulations have shown that electrostatics in this region is of importance.[67] Furthermore, previous work by Monticelli has showed that it is far from trivial to exactly reproduce atomistic PMFs with CG models.[68] Given

dx.doi.org/10.1021/ct400466m | J. Chem. Theory Comput. 2014, 10, 5−13

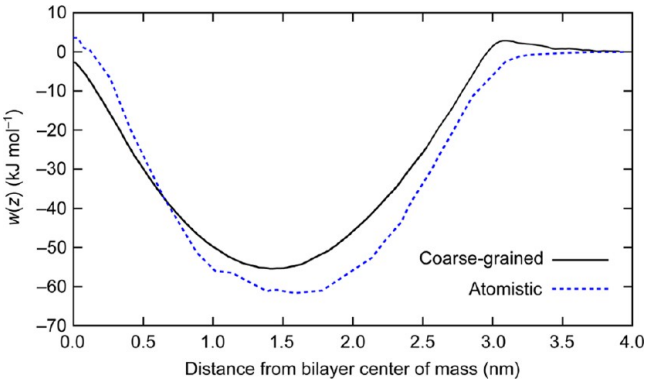

Figure 3. Potential of mean force (PMF), $w(z)$, of transferring a hypericin molecule from bulk water to the middle of a DPPC lipid bilayer at 323 K. The atomistic PMF is taken from a previous study[23] and the coarse-grained one from the current work.

the relatively small differences in the two PMFs, we can conclude that the current CG model of hypericin is of satisfactory quality and therefore can be used for large scale studies like the ones presented below.

In order to further verify our CG model of hypericin, US simulations of two hypericin molecules in aqueous phase were conducted in both atomistic and CG resolution. The atomistic simulations were performed in an analogous fashion to our previous work.[23] The reaction coordinate was the COM distance between the two solutes. Each umbrella window had a separation of 0.07−0.08 nm, and a force constant of 1000 kJ mol^{-1} nm^{-2} was used. The atomistic simulations were run for 100 ns per window, and the CG simulations for 250 ns per window. As the volume available for hypericins is gradually increased along the reaction coordinate, an analytical entropy correction was added to the PMF according to

$$T\Delta S_{r_0}(r) = 2k_B T \ln\left(\frac{r}{r_0}\right) \quad (1)$$

where k_B is the Boltzmann constant, T the absolute temperature, and r_0 = 0.35 nm. In Figure 4, the resulting PMFs are compared, and it is clear the CG reproduces the shape of the atomistic PMF relatively well, only showing a slightly too pronounced affinity at longer distance. Qualitatively

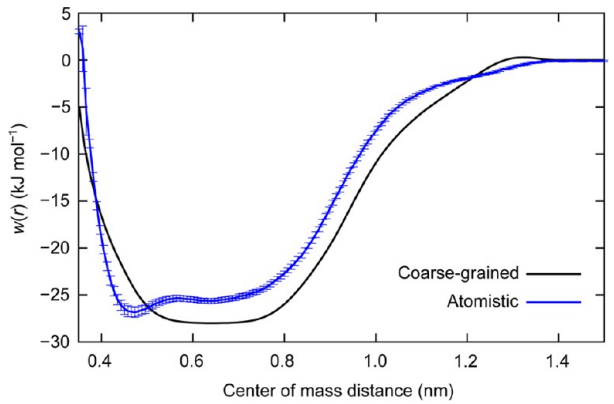

Figure 4. Free energy profile of bringing two hypericin molecules together with both an atomistic model and coarse-grained model derived in the current work. The error bars for the coarse-grained profile is within the line width.

speaking, the PMFs are not in excellent agreement, but as observed by de Jong et al.,[69] it can be difficult to obtain perfect correspondence between atomistic and CG models. In our CG simulations, the intermolecular interactions between hypericin molecules are too strong. However, it should be mentioned that these PMFs were not used for the actual parametrization, so the comparison offers a way to validate our model. The shapes of the PMFs also differ. The minima around 0.45 nm for the atomistic simulations is not observed for CG model, and the increase in free energy starts at a longer distance for the CG model. As in the case of the lipid bilayer, there may be several reasons for these differences. It is plausible that the water model (basically a Lennard−Jones model) of Martini causes this due to the lack of electrostatic interactions. The water beads used in Martini consist of four water molecules. At short hypericin−hypericin distances, we can thus assume that the beads are too large and thus do not satisfactory represent a situation with fewer water molecules occupying the space between the two molecules. Further, it would be difficult to reproduce the intermolecular hydrogen bonds that could be formed between two hypericin molecules with a CG model. As it is clear that two hypericins form a dimer with both models, we keep our CG model but note that there may be room for future improvements.

Lipid Bilayer Simulations. Besides comparing the CG PMF to the UA PMF, one can also validate the newly derived CG model by looking at structural distributions such as tilt angles.[59] In order to do this, two CG hypericin molecules were placed in a lipid bilayer (one in each leaflet) consisting of 256 DPPC lipids hydrated with 4096 water beads. The simulations lasted for 2.5 μs with the same settings as described earlier, and the UA data was taken from earlier work.[23] First, the angle between the vector connecting beads R8 and R9 to the membrane normal was analyzed, and the results are presented in Figure 5a. An angle of 0° corresponds to a geometry where the hypericin is perfectly aligned with the vector orthogonal to the membrane surface, and an angle of 90° corresponds to the geometry where these vectors are perpendicular. There are some differences in the angle distributions, and they both range from 0 to 80−90°. For the CG model, the distributions is wider, indicating a larger orientational freedom, and the maximum is located at a larger angle than that observed with the UA model. As the CG simulations were more elaborate than the UA simulations in terms of length (2.5 μs vs 50 ns), it is possible that the UA simulations have not been able to properly sample every thermally accessible state. The convergence of molecular tilts in lipid bilayers have been shown to require extensive sampling.[59,70]

Another structural feature of interest is the angle between the vector normal to the molecular plane of hypericin and the membrane normal; the distribution of this angle for the CG simulations are compared to the previous UA simulations in Figure 5b. The agreement between the two models is very high. For the CG model, the distribution is slightly wider but not to any noticeable extent. The maxima around 90° means that the plane is aligned parallel to the membrane normal, and together with the previous distribution, it is clear that the molecule orients itself with the less polar end (beads R2, R7, R8, and R5) toward the center of the membrane and with the beads of a more polar nature (ROH, R10, R9, and R6) toward the water, in agreement with experiments.[71] This is also seen in Figure 6, where the distance between these two entities and the lipid bilayer COM is plotted. In agreement with chemical intuition,

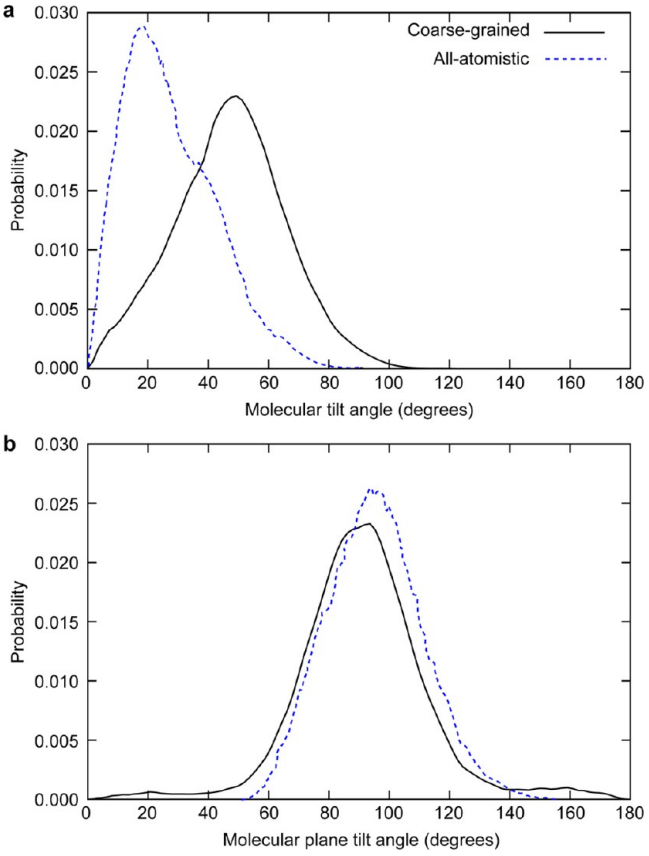

Figure 5. (a) Distributions of the angles between the vector spanning from R8 to R9 and the vector normal to the lipid bilayer. (b) Angle between the bilayer normal and the vector normal to the molecular plane of hypericin. The coloring in (b) is the same as in (a).

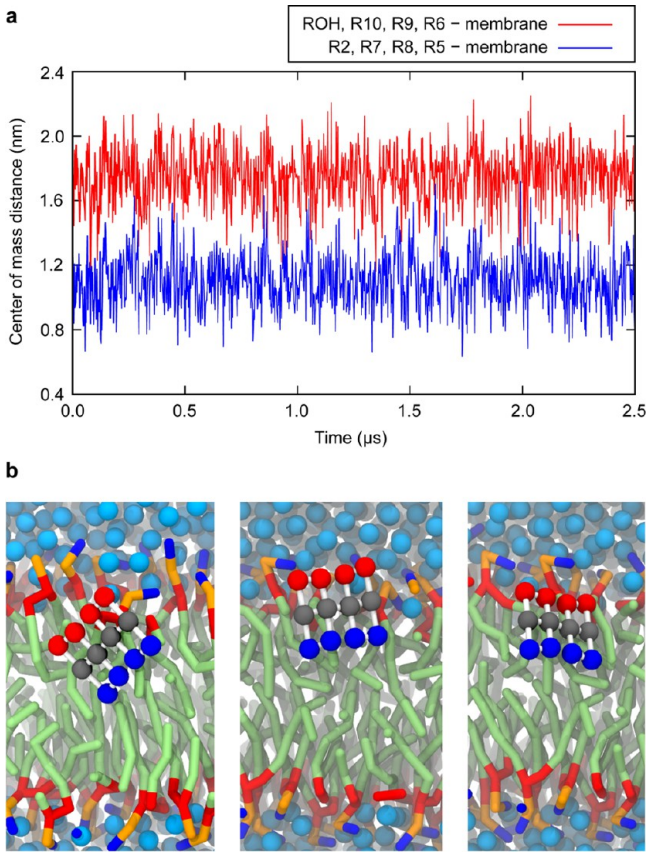

Figure 6. (a) Center of mass distance between selected parts of the hypericin molecule and a DPPC lipid bilayer; the more polar end (ROH, R10, R9, R6 – membrane) in red and the less polar end (R2, R7, R8, R5 – membrane) in blue. (b) Snapshots from the simulation illustrating the orientation of hypericin. The coloring in (b) is the same as in (a).

the less polar end thus tries to minimize its contact with the aqueous surrounding.

Overall, we can summarize the analysis of the CG bilayer simulations by concluding that the agreement between the CG and UA models is good and that the CG model is able to reproduce most characteristics of the UA model despite the lack of explicit electrostatic interactions. The balance between hypericin's hydrophilic and hydrophobic sides is captured well, providing confidence in the model to be used in the larger liposome simulations.

Liposome Simulations. As the CG model of hypericin was shown to reproduce the essential features in the interaction between the photosensitizing drug and lipids, large scale simulations of a liposome with different amounts of hypericin were performed. In the two following sections, these simulations are discussed.

Structure of the Liposome. The inner and outer radii, $\bar{r}_{inner}$ and $\bar{r}_{outer}$, of the liposome were defined as the average distance between the phosphate groups of the lipids in their corresponding monolayer and the COM of the liposome. Figure S1 of the Supporting Information displays how these values fluctuate with time. In general, the differences between the simulations are small; the fluctuations in $\bar{r}_{outer}$ are slightly smaller for the simulations with the highest amount of hypericin. Clearly, the liposomes are stable during the simulations as no extreme fluctuations or changes in size are visible during the 10 μs long simulations, and the effects of adding hypericin appear to be relatively small also when added to the center of the liposome. In Table 2, the average radii are presented along with the area per lipid for the inner and outer monolayer. The change in area per lipid is evident, especially for the inner monolayer where it increases by 0.02 nm^2 when going from a hypericin-free system to the highest concentration. In accordance with experimental studies, the size of the liposome is increased with a higher hypericin concentration.[72] The expansion of the liposome is straightforward to rationalize; as the hypericin molecules and aggregates penetrate the liposome, this has to expand in order to embed the drug molecules.

It is important to note that the areas per lipid have been calculated using the simple geometric relationship $A^L = 4\pi\bar{r}^2/n$, where n is the number of lipids in the inner/outer monolayer; hence, the area taken up by hypericin is not accounted for. As the larger aggregates tend to stay on the lipid surface and only a small portion of them actually penetrates into the bilayer, we believe that this approximation is justified. The difference between our simulation scales and most experimental scales should also be mentioned; the liposomes studied here are about 3 times smaller than the smallest systems studied in experiments. Hence, differences between our simulations and experiments could, for example, stem from differences in curvature.

Distribution of Hypericin in Liposomes. With the aim to illustrate the hypericin distributions, radial distribution functions (RDFs) between the COM of the liposome and

dx.doi.org/10.1021/ct400466m | J. Chem. Theory Comput. 2014, 10, 5–13

Table 2. Radius of Spheres Made Up by Inner and Outer Lipid Layers in Liposome, $\bar{r}_{inner}$ and $\bar{r}_{outer}$, Respectively, and Their Corresponding Area per Lipid $(A^L)^{ba}$

system	$\bar{r}_{inner}$ (nm)	$\bar{r}_{outer}$ (nm)	A^L_{inner} (nm^2)	A^L_{outer} (nm^2)
no hypericin	6.24 ± 0.62	10.15 ± 0.65	0.517 ± 0.05	0.819 ± 0.05
21 hypericin[c]	6.31 ± 0.68	10.02 ± 0.70	0.528 ± 0.04	0.798 ± 0.05
21 hypericin	6.30 ± 0.60	10.12 ± 0.58	0.527 ± 0.05	0.814 ± 0.03
42 hypericin	6.29 ± 0.66	10.13 ± 0.72	0.525 ± 0.06	0.816 ± 0.07
64 hypericin	6.36 ± 0.72	10.19 ± 0.71	0.537 ± 0.06	0.825 ± 0.06
84 hypericin	6.36 ± 0.73	10.23 ± 0.74	0.537 ± 0.07	0.831 ± 0.07

[a]Errors were computed using block-averaging. [b]$A^L = 4\pi\bar{r}^2/n$; n is the number of lipids in the corresponding monolayer. [c]One hypericin in the middle.

selected parts of the lipids and hypericin were calculated; the results are shown in Figure 7a (see the Supporting Information

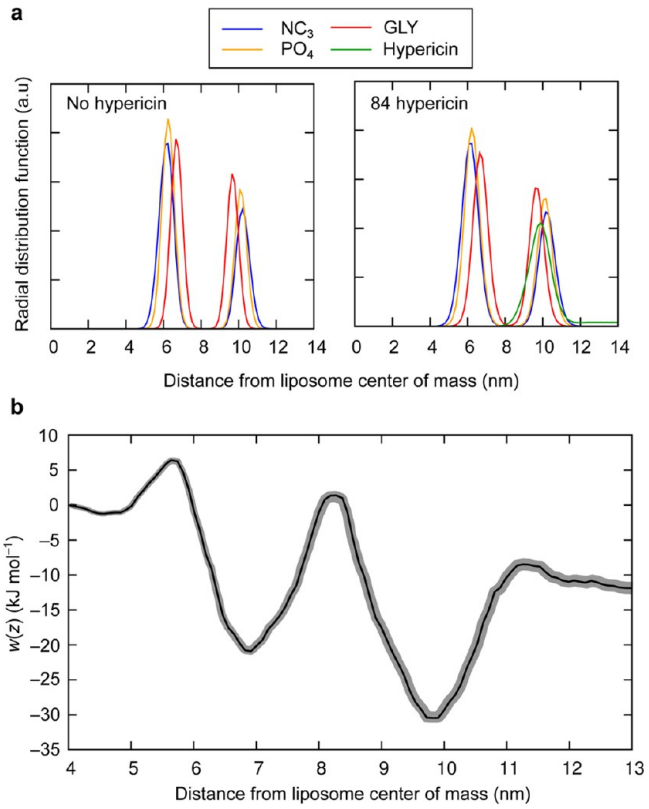

Figure 7. (a) Radial distribution functions between the center of mass of the liposome and selected moieties. (b) Potential of mean force (black line) with the statistical error (gray area) for transferring a single hypericin across the lipids in a liposome.

for the remaining RDFs). As expected from the PMF in Figure 3, hypericin penetrates the lipids down to the glycerol region in the outer monolayer, and the partitioning at the interface between the lipid/water interface is in agreement with experimental work of Losi[73] and Weitman et al.,[74] where the same preferred location was observed. When the concentration is increased, the peak of the hypericin distribution is moved slightly toward the aqueous phase (Figure 7a and Figure S1, Supporting Information). For the simulations that had one hypericin in the middle of the liposome (label 21 hypericin*, Figure S1, Supporting Information), it is clear from the small peak at a distance of roughly 7 nm from the liposome COM that also the inner hypericin penetrates the lipid surface and prefers to be buried around the glycerol region of the lipids.

To bring further understanding to the differences in interactions between the lipids and hypericin in the inner and outer monolayer, the PMF of transferring a hypericin from the inside to the outside of the liposome was constructed. The PMF was constructed following the procedure described earlier with only a shorter a sampling time; each US window was sampled for 100 ns. In Figure 7b, the results are presented, and the overall shape of the PMF can be compared to the membrane simulations reported in Figure 3. The differences between the free energy of transferring the molecule from the center of the liposome to the inner and outer monolayer are most evident in well depth and the barrier at the surface of the lipids. For the inner monolayer, the barrier of penetration is higher, and the well depth is shallower compared to the outer monolayer, which is likely caused by the curvature of the inner lipids. In order for the liposome to maintain its shape, the inner lipids have to pack much tighter than the outer ones, and hence, a large negative curvature is obtained. This high density region is more difficult for hypericin to penetrate compared to the less dense lipid surface of the outer monolayer. The height of the barrier of transferring hypericin from the inner to the outer layer is also lower compared to the opposite transfer for the exact same reason. There is also a difference between the two aqueous phases: the confined water inside the liposome and the bulk water. This can be rationalized by the fact that these two phases have differently. The confined water is clearly different from the bulk water, and hence, the solvation free energies in these two solvents will differ.

The distribution and aggregation of hypericin in the studied systems are shown in Figure 8. The clustering of hypericin is very evident at higher concentrations, and relatively large aggregates are formed. This is in qualitative agreement with experiments,[75] where fluorescence measurements showed that hypericin indeed forms aggregates, which can be rationalized by the π-stacking between the aromatic cores of the molecules. It is quite remarkable that a CG model with three or four heavy atoms per bead is able to show this feature. As mentioned earlier, the larger aggregates are unable to penetrate the liposome but tend to stick to the surface or penetrate the surface with the outermost molecules of the "worm-like" stacked structure. Once an aggregate is formed, it stays intact during the time scales simulated here. It is of interest to study whether these aggregates are able to be delivered by the liposome or if it is the monomers or smaller aggregates of hypericin that are being transferred to the cell. It could be that the free energy barrier of transferring a large aggregate from the host liposome to the targeting cell is lower than transferring a single hypericin molecule that is buried within the liposome. However, because dimerized hypericin cannot form singlet oxygen,[76] the photodynamic action is thus affected by the

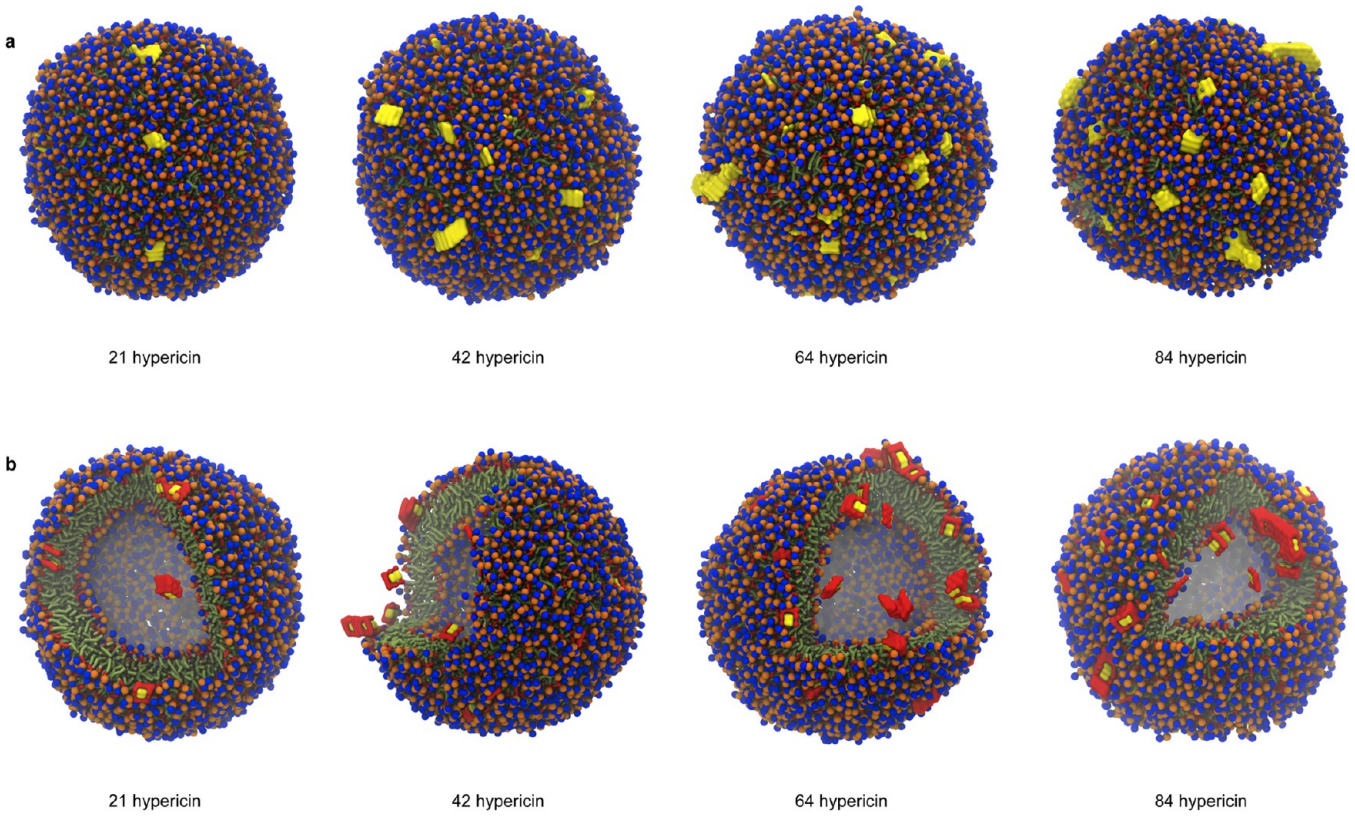

Figure 8. (a) Final snapshots from the 10 μs molecular dynamics simulations of liposomes (coloring is the same as in Figure 1) loaded with hypericin molecules (in yellow). (b) Snapshots with some lipids removed in order to illustrate the binding of hypericin; the hydrophilic parts of hypericin are shown in red and the hydrophobic parts in yellow.

aggregation. It is therefore crucial that the molecules are delivered in the monomeric form to the tumor tissues. Future work in our group aim at elucidating the transfer mechanism of hypericin from the host liposome to a target membrane. Another direction of future work is to perform multi-scale simulations of the systems.[77,78] In these simulations, selected parts of the systems are treated at higher resolution, and the rest of the system is treated by a CG representation. This could prove to be important in, for example, the interaction between a liposome and a model membrane because it has been shown that the merging process may be governed by individual lipids,[21] and the role of confined water is not to be ignored.[22]

CONCLUSIONS

A CG model of the photosensitizing drug hypericin has been developed following the Martini CG scheme. The target data was taken from a previous UA study.[23] The newly derived CG model showed good agreement with observables obtained from the atomistic simulations. Further, simulations performed on the microsecond time scale of liposomes with varying hypericin concentration showed that the liposome expands as the amount of hypericin is increased, which is in agreement with experimental work. The effects of hypericin on the liposome besides this small expansion are minor at the concentrations used here, and no major structural differences could be pointed out. The hypericins are mainly found close to the polar headgroup region of the outer lipid layer and orient so as to maximize the interactions at their more hydrophobic (toward lipid interior) and hydrophilic ends (toward water phase). We further note that the hypericins tend to aggregate through π-stacking, especially at the higher drug loading, with only a few of the hypericins penetrating into the lipid bilayer. This aggregation phenomenon has also been noted experimentally in aqueous solution.[75,79] PMF calculations of pulling a hypericin from the interior water phase of the liposome through the lipid wall to the exterior water phase display a clear difference in well depth between the inner and outer layer. The barrier to penetration of the inner layer is higher and the well more shallow, and it is plausible that the differences in curvature and lipid density of the inner and outer layer is the cause of this.

The presented results show that the current CG model of hypericin can be used in large-scale studies where the actual mechanism of drug delivery from a liposome to a membrane can be studied using CG-MD. If questions regarding how this type of drug delivery is facilitated can be answered at near atomistic resolution, they will bring further insight into how to optimize systems for delivery to certain physiological regions or to target specific cell types.

ASSOCIATED CONTENT

Supporting Information

Figures showing the evolution of the liposome radius and radial distribution functions at different hypericin loadings. A zip archive contains Gromacs topologies and force field parameters for hypericin along with coordinates for a equilibrated liposome containing 2528 DPPC lipids. This material is available free of charge via the Internet at http://pubs.acs.org.

AUTHOR INFORMATION

Corresponding Author

*E-mail: leif.eriksson@chem.gu.se.

Notes

The authors declare no competing financial interest.

■ ACKNOWLEDGMENTS

The Faculty of Science at the University of Gothenburg and the Swedish science research council are acknowledged for financial support. Grants of computing time from the Swedish National Infrastructure Committee (SNIC) are gratefully acknowledged, as is support from the "COST Action CM1002 COnvergent Distributed Environment for Computational Spectroscopy (CODECS)".

■ REFERENCES

(1) Cerny, C. Z. *Phys. Chem.* **1911**, *73*, 371−382.
(2) Chung, P. S.; Rhee, C. K.; Kim, K. H.; Paek, W.; Chung, J.; Paiva, M. B.; Eshraghi, A. A.; Castro, D. J.; Saxton, R. E. *Laryngoscope* **2000**, *110*, 1312−1316.
(3) Chen, B.; Xu, Y.; Roskams, T.; Delaey, E.; Agostinis, P.; Vandenheede, J. R.; de Witte, P. A. *Int. J. Cancer* **2001**, *93*, 275−282.
(4) Chen, B.; de Witte, P. A. *Cancer Lett.* **2000**, *150*, 111−117.
(5) Thomas, C.; Pardini, R. S. *Photochem. Photobio. Sci.* **1992**, *55*, 831−837.
(6) VanderWerf, Q. M.; Saxton, R. E.; Chang, A.; Horton, D.; Paiva, M. B.; Andersson, J.; Foote, C.; Soudant, J.; Mathey, A.; Castro, D. J. *Laryngoscope* **1996**, *106*, 479−483.
(7) Andreoni, A.; Colasanti, A.; Colasanti, P.; Mastrocinque, M.; Riccio, P.; Roberti, G. *Photochem. Photobiol. Sci.* **1994**, *59*, 529−533.
(8) Lopezbazzocchi, I.; Hudson, J. B.; Towers, G. H. N. *Photochem. Photobiol. Sci.* **1991**, *54*, 95−98.
(9) Lenard, J.; Rabson, A.; Vanderoef, R. *Proc. Natl. Acad. Sci. U.S.A.* **1993**, *85*, 158−162.
(10) Meruelo, D.; Lavie, G.; Lavie, D. *Proc. Natl. Acad. Sci. U.S.A.* **1988**, *85*, 5320−5234.
(11) Moraleda, G.; Wu, T. T.; Jilbert, A. R.; Aldrich, C. E.; Condreay, L. D.; Larsen, S. H.; Tang, J. C.; Colacino, J. M.; Mason, W. S. *Antiviral Res.* **1993**, *20*, 235−247.
(12) Senthil, V.; Jones, L. R.; Senthil, K.; Grossweiner, L. I. *Photochem. Photobiol. Sci.* **1994**, *59*, 40−47.
(13) Chaloupka, R.; Obsil, T.; Plasek, J.; Sureau, F. *Biochim. Biophys. Acta* **1999**, *1418*, 39−47.
(14) Mukheriee, P.; Adhikary, R.; Halder, M.; Petrich, J. W.; Miskovsky, P. *Photochem. Photobiol. Sci.* **2008**, *84*, 706−712.
(15) Kascakova, S.; Refregiers, M.; Jancura, D.; Sureau, F.; Maurizot, J. C.; Miskovsky, P. *Photochem. Photobiol. Sci.* **2005**, *81*, 1395−1403.
(16) Torchilin, V. P. *Nat. Rev. Drug Discovery* **2005**, *4*, 145−160.
(17) Samad, A.; Sultana, Y.; Agil, M. *Curr. Drug Delivery* **2007**, *4*, 297−305.
(18) Kępczyński, M.; Nawalany, K.; Jachimska, B.; Romek, M.; Nowakowska, M. *Colloids Surf., B* **2006**, *49*, 22−30.
(19) Sibani, S. A.; McCarron, P. A.; Woolfson, A. D.; Donnelly, R. F. *Expert Opin. Drug Delivery* **2008**, *5*, 1241−1254.
(20) de Vries, A. H.; Mark, A. E.; Marrink, S. J. *J. Am. Chem. Soc.* **2004**, *126*, 4488−4489.
(21) Kasson, P. M.; Lindahl, E.; Pande, V. S. *PLoS Comput. Biol.* **2010**, *6*, e1000829.
(22) Kasson, P. M.; Lindahl, E.; Pande, V. S. *J. Am. Chem. Soc.* **2011**, *133*, 3812−3815.
(23) Eriksson, E. S. E.; Santos, D. J. V. A. d.; Guedes, R. C.; Eriksson, L. A. *J. Chem. Theory Comput.* **2009**, *5*, 3139−3149.
(24) Eriksson, E. S. E.; Eriksson, L. A. *J. Chem. Theory Comput.* **2011**, *7*, 560−574.
(25) Murtola, T.; Bunker, A.; Vattulainen, I.; Deserno, M.; Karttunen, M. *Phys. Chem. Chem. Phys.* **2009**, *11*, 1869−1892.
(26) Marrink, S. J.; Risselada, H. J.; Yefimov, S.; Tieleman, D. P.; de Vries, A. H. *J. Phys. Chem. B* **2007**, *111*, 7812−7824.
(27) Marrink, S. J.; de Vries, A. H.; Mark, A. E. *J. Phys. Chem. B* **2004**, *108*, 750−760.
(28) López, C. A.; Sovova, Z.; van Eerden, F. J.; de Vries, A. H.; Marrink, S. J. *J. Chem. Theory Comput.* **2013**, *9*, 1694−1708.
(29) Monticelli, L.; Kandasamy, S. K.; Periole, X.; Larson, R. G.; Tieleman, D. P.; Marrink, S.-J. *J. Chem. Theory Comput.* **2008**, *4*, 819−834.
(30) de Jong, D. H.; Singh, G.; Bennett, W. F. D.; Arnarez, C.; Wassenaar, T. A.; Schäfer, L. V.; Periole, X.; Tieleman, D. P.; Marrink, S. J. *J. Chem. Theory Comput.* **2013**, *9*, 687−697.
(31) López, C. A.; Rzepiela, A. J.; de Vries, A. H.; Dijkhuizen, L.; Hünenberger, P. H.; Marrink, S. J. *J. Chem. Theory Comput.* **2009**, *5*, 3195−3210.
(32) Marrink, S. J.; Mark, A. E. *J. Am. Chem. Soc.* **2003**, *125*, 15233−15242.
(33) Marrink, S. J.; Mark, A. E. *J. Am. Chem. Soc.* **2003**, *125*, 11144−11145.
(34) Louhivuori, M.; Risselada, H. J.; van der Giessen, E.; Marrink, S. J. 2010, *107*, 19856−19860.
(35) Risselada, H. J.; Marrink, S. J. *Phys. Chem. Chem. Phys.* **2009**, *11*, 2056−2067.
(36) Risselada, H. J.; Marrink, S. J. *Proc. Natl. Acad. Sci. U.S.A.* **2008**, *105*, 17367−17372.
(37) Schäfer, L. V.; Marrink, S. J. *Biophys. J.* **2010**, *99*, L91−L93.
(38) Schäfer, L. V.; de Jong, D. H.; Holt, A.; Rzepiela, A. J.; de Vries, A. H.; Poolman, B.; Killian, J. A.; Marrink, S. J. *Proc. Natl. Acad. Sci. U.S.A.* **2011**, *108*, 1343−1348.
(39) Arnarez, C.; Mazat, J.-P.; Elezgaray, J.; Marrink, S. J.; Periole, X. *J. Am. Chem. Soc.* **2013**, *135*, 3112−3120.
(40) Periole, X.; Knepp, A. M.; Sakmar, T. P.; Marrink, S. J.; Huber, T. *J. Am. Chem. Soc.* **2012**, *134*, 10959−10965.
(41) Domański, J.; Marrink, S. J.; Schäfer, L. V. *Biochim. Biophys. Acta* **2012**, *1818*, 984−994.
(42) Tozzini, V. *Curr. Opin. Struct. Biol.* **2005**, *15*, 144−150.
(43) Wang, Z.-J.; Deserno, M. *J. Phys. Chem. B* **2010**, *114*, 11207−11220.
(44) Bereau, T.; Deserno, M. *J. Chem. Phys.* **2009**, *130*, 235106.
(45) Saunders, M. G.; Voth, G. A. *Curr. Opin. Struct. Biol.* **2012**, *22*, 144−150.
(46) Basdevant, N.; Borgis, D.; Ha-Doung, T. *J. Chem. Theory Comput.* **2012**, *9*, 803−813.
(47) Pasi, M.; Lavery, R.; Ceres, N. *J. Chem. Theory Comput.* **2013**, *9*, 785−793.
(48) Izvekov, M.; Parrinello, S.; Burnham, C. J.; Voth, G. A. *J. Chem. Phys.* **2004**, *120*, 10896−10913.
(49) Noid, W. G.; Chu, J. W.; Ayton, G. S.; Krishna, V.; Izvekov, S.; Voth, G. A.; Das, A.; Andersen, H. C. *J. Chem. Phys.* **2008**, *128*, 244144.
(50) Lyubartsev, A. P.; Laaksonen, A. *Phys. Rev. E* **1995**, *52*, 3730−3737.
(51) Lyubartsev, A.; Mirzoev, A. P.; Chen, L.; Laaksonen, A. *Faraday Discuss.* **2010**, *144*, 43−65.
(52) Jochum, M.; Andrienko, D.; Kremer, K.; Peter, C. *J. Chem. Phys.* **2012**, *137*, 064102.
(53) Becke, A. D. *J. Chem. Phys.* **1993**, *98*, 5648−5652.
(54) Lee, C.; Wang, W.; Parr, R. G. *Phys. Rev. B* **1988**, *37*, 785−789.
(55) Vosko, S. H.; Wilk, L.; Nusair, M. *Can. J. Phys.* **1980**, *58*, 1200−1211.
(56) Stephens, P. J.; Devlin, F. J.; Chabalowski, C. F.; Frisch, M. J. *J. Phys. Chem.* **1994**, *98*, 11623−11627.
(57) Eriksson, E. S. E.; Guedes, R. C.; Eriksson, L. A. *Int. J. Quantum Chem.* **2008**, *118*, 1921−1929.
(58) Torrie, G. M.; Valleau, J. P. *J. Comput. Phys.* **1977**, *23*, 187−199.
(59) Hinner, M. J.; Marrink, S. J.; de Vries, A. H. *J. Phys. Chem. B* **2009**, *113*, 15807−15819.
(60) Neale, C.; Bennett, W. F. D.; Tieleman, D. P.; Pomès, R. *J. Chem. Theory Comput.* **2011**, *7*, 4175−4188.
(61) Kumar, S.; Bouzida, D.; Swendsen, R. H.; Kollman, P. A.; Rosenberg, J. M. *J. Comput. Chem.* **1992**, *13*, 1011−1021.
(62) Hess, B.; Kutzner, C.; van der Spoel, D.; Lindahl, E. *J. Chem. Theory Comp.* **2008**, *4*, 435−447.

(63) Berendsen, H. J. C.; Postma, J. P. M.; van Gunsteren, W. F.; DiNola, A.; Haak, J. R. *J. Chem. Phys.* **1984**, *81*, 3684−3690.
(64) Winger, M.; Trzesniak, D.; Baron, R.; van Gunsteren, W. F. *Chem. Phys. Phys. Chem.* **2009**, *11*, 1934−1941.
(65) Marrink, S. J.; Periole, X.; Tieleman, D. P.; de Vries, A. H. *Chem. Phys. Phys. Chem.* **2009**, *12*, 2254−2256.
(66) Martínez, L.; Andrade, R.; Birgin, E. G.; Martínez, E. G. *J. Comput. Chem.* **2009**, *30*, 2157−2164.
(67) Jämbeck, J. P. M.; Lyubartsev, A. P. *Phys. Chem. Chem. Phys.* **2013**, *15*, 4677−4686.
(68) Monticelli, L. *J. Chem. Theory Comput.* **2012**, *8*, 1370−1378.
(69) de Jung, D. H.; Periole, X.; Marrink, S. J. *J. Chem. Theory Comput.* **2012**, *8*, 1003−1014.
(70) Monticelli, L.; Tieleman, D. P.; Fuchs, P. F. J. *Biophys. J.* **2010**, *99*, 1455−1464.
(71) Strejčková, A.; Staničová, J.; Jancura, D.; Miškovský, P.; Báná, G. *J. Phys. Chem. B* **2013**, *117*, 1280−1286.
(72) Cohen, Y.; Weitman, H.; Afri, M.; Yanus, R.; Rudnick, S.; Talmon, Y.; Schmidt, J.; Aped, P.; Shatz, S.; Ehrenberg, B.; Frimer, A. A. *J. Liposome Res.* **2012**, *22*, 306−318.
(73) Losi, A. *Photochem. Photobiol.* **1997**, *65*, 791−801.
(74) Weitman, H.; Roslaniec, M.; Frimer, A. A.; Afri, M.; Freeman, D.; Mazur, Y.; Ehrenberg, B. *Photochem. Photobiol.* **2001**, *73*, 110−118.
(75) Bánó, G.; Staničová, J.; Jancura, D.; Marek, J.; Bánó, M.; Uličný, J.; Strejčková, A.; Miškovský, P. *J. Phys. Chem. B* **2011**, *115*, 2417−2423.
(76) Burel, L.; Jardon, P. *J. Chim. Phys.* **1996**, *93*, 300−316.
(77) Rzepiela, A. J.; Schäfer, L. V.; Goga, N.; Risselada, H. J.; De Vries, A. H.; Marrink, S. J. *J. Comput. Chem.* **2010**, *31*, 1333−1343.
(78) Wassenaar, T. A.; Ingolfsson, H.; Prieß, M.; Marrink, S. J.; Schäfer, L. V. *J. Phys. Chem. B* **2013**, *117*, 3516−3530.
(79) Roslaniec, M.; Weitman, H.; Freeman, D.; Mazur, Y.; Ehrenberg, B. *J. Photochem. Photobiol. B* **2000**, *57*, 149−158.